Global Scientific JOURNALS

GSJ: Volume 9, Issue 2, February 2021, Online: ISSN 2320-9186
www.globalscientificjournal.com

STUDY OF THE EFFECT OF ANNEALING TEMPERATURE ON Zn DOPED TiO_2 NANOCRYSTAL STRUCTURES PREPARED BY SOL-GEL METHOD

Rabin Siwakoti[1], Dr. Suresh Kumar Dhungel[2], Dr. Surendra Kumar Gautam[1], Sanjit karki[1], Kebindra Shrestha[1], Prashanta sharma[3]

1. Department of Chemistry, Tri- Chandra Multiple Campus, Tribhuvan University, Kathmandu

2. Nepal Academy of Science and Technology- NAST, Khumaltar, Lalitpur

3. Department of Chemistry, Amrit Campus, Tribhuvan University, Kathmandu

Keywords: Zinc doped TiO_2, Photo-catalysis, Sol- Gel method, Phase transformation of TiO_2, titania nanoparticles, SEM analysis, Debye- Scherrers formula

ABSTRACT

The advancement of TiO_2 has always been serious concern for the better performance of photo-catalytic behavior even in unsuitable intensity of light. For this issue, the doping of TiO_2 with transition metals has attracted serious attention for the researchers. Zn^{2+} metal ion is more effective among other transition metal ions such as Fe^{2+}, Mn^{2+}, Cu^{2+}, Zn^{2+} etc., because the ionic radii of Zn^{2+} (0.074 nm) and of Ti^{4+} (0.075 nm) are similar to each other and hence, it is easier

for substituting Ti^{4+} ion by Zn^{2+} ion without destroying crystal structure. For the preparation of zinc ion doped titania nanoparticles very useful Sol- Gel synthesis tool has been used during this research. Zn^{2+} ion was doped on titania varying the concentration of Zn^{2+} (from 0.1 M to 0.5 M). The prepared samples were characterized by XRD and SEM tools. The prepared samples were found to be having 7 nm average grain size after the determination of sample diameter by applying Debye- Scherrers formula. While the XRD data for specific sample (A_2), of which SEM analysis was carried out, was found to be 12.32 nm and was supported by the information derived from SEM (11.90 nm). On comparison between annealing temperature and size of nanocrystals, it was found that on increasing annealing temperature the crystal size also increases gradually. The variation in annealing temperature above 500^0C results in the transformation of anatase TiO_2 crystals into rutile crystals.

1. Introduction

1.1 Titanium Dioxide (TiO_2)

Titanium dioxide, also known as Titanium (IV) oxide, was first discovered in 1821 and is one of the top 20 inorganic chemicals of industrial importance. It does not occur in nature itself but derived from ilmenite ore. Not only tetravalent but also divalent (TiO) and trivalent (Ti_2O_3) states of oxides of titanium are also reported in some compounds [1]. It is a most preferred semiconductor photo catalytic material due to its favorable properties like non- toxicity, chemical inertness, and stability over a pH range [2].

The important characteristics of TiO_2 are:

- It is amphoteric in nature.
- Insoluble in water as well as acids.

1.1.1 Applications TiO_2 nanoparticles

TiO_2 nanoparticles are applied in the formation of dye sensitized solar cells which is composed of porous layer of TiO_2 NPs, covered with a molecular dye that absorbs sunlight as chlorophyll

in plant leaves. The dye molecules are of nanometric size in solar cells, in order to capture a reasonable amount of incoming light a thick layer of dye is needed. To solve this problem, a semiconductor nanomaterial (TiO_2) is used as a scaffold to hold large number of dye molecules in a 3-D matrix by increasing the number of molecules for any given surface area of solar cell [3, 4]. TiO_2 has higher resistance towards corrosion and body fluids which makes it more biocompatible for its pharmaceutical uses. Compared to other materials, it is more suitable for orthopedic treatment due to its high specific strength and low elastic modulus. It also has lower density than other metallic biomaterials so that titanium implants are lighter than stainless steel implanting [5]. Metal doped TiO_2 nanoparticles are also being used in the manufacture of self-cleaning smart textiles. When TiO_2 absorbs light with more than its band gap, electron gets excited to the conduction band and positively charged holes remain in the valence band. These excited electrons react with absorbed oxygen to form superoxide ions. The positive holes in valence band react with water and form hydroxide radical. These hydroxide radicals oxidize different organic contaminants into CO_2 and water.

1.1.2 Crystalline structure of TiO_2 nanoparticles

Titanium dioxides are found in crystalline as well as amorphous forms. The crystalline forms of titanium are Anatase, Rutile, and Brookite. Each crystalline forms exhibit specific characters such as band gap, surface states etc. differing in their applications. Anatase and rutile are well known photo- catalysts with anatase generally showing much higher photo- catalytic activity. Rutile is commonly used as a white pigment in paints and brookite is not yet of commercial interest but a Dye sensitized solar cells (DSSC) has been reported [6]. Anatase and rutile are both tetragonal in structure while the brookite structure is orthorhombic. In case of all the crystalline forms, each Ti^{4+} ions are surrounded by an irregular octahedron of oxide ions. In the rutile crystal each octahedron is in contact with 10 neighbor octahedrons (2 sharing edge oxygen pairs and 8 sharing corner oxygen atoms), while in anatase each octahedron is in contact with eight

neighbors (4 sharing an edge and 4 sharing a corner). The octahedral linkage in brookite is such that the three edges are shared per octahedron [7, 8]. The structure of rutile and anatase can be described in terms of chains of [TiO_6] octahedral, where each Ti^{4+} ion is surrounded by an octahedron of six O^{2-} ions. The two crystal structures i.e. anatase and rutile often differ in distortion of each octahedron and by the assembly pattern of octahedral chains. The octahedron in rutile is not regular, showing slight orthorhombic distortion while the octahedron in anatase is significantly distorted so that its symmetry is lower than orthorhombic [9, 10].

1.1.3 Phase transformation: anatase to rutile

The transformation behavior from amorphous TiO_2 to anatase or anatase to rutile phases is influenced by the synthesis environment. The various factors affecting the phase transformation are temperature, pressure, particle diameter, dopant, and hydrothermal conditions.

1.1.3.1 Temperature:

The amorphous titania converts into a crystalline anatase structure under the heat treatment below 400^0C, which when further heated above 600^0C converts into rutile titania. [11] The transformation from anatase to rutile phase is also the transformation from meta-stable to stable state. However, no unique phase transformation temperature is reported, the anatase to rutile phase transformation occurs in the temperature range of 600^0C – 800^0C [12]. The direct transformation of brookite to rutile can be observed above 700^0C temperature [13].

1.1.3.2 Dopants:

The anatase to rutile phase transformation depends upon the kind of the cation (Li^+, K^+, Zn^{2+}, Al^{3+}) used to dope the TiO_2 powders. The phase transition occurs at different temperature according to the different metal ions used as dopants. The anatase phase of TiO_2 can be stabilized by the presence of additives such as alumina, silica, zirconia, sulphate ions etc. whereas chloride ions shows accelerating effect on the anatase to rutile phase transformation under hydrothermal conditions [14, 15]. The mechanism by which the additives inhibit or

promote the anatase to rutile phase transformation is influenced by the defect of structure of titania i.e., the concentration of oxygen vacancies or Ti interstitials. The oxygen deficiency facilitate the anatase- rutile phase transition however, some additives retard the transformation by increasing lattice defects of titania [16].

1.2 Preparation of Nanoparticles

There are two methods for synthesis of nanoparticles, namely top down technique and bottom up technique. Top down method includes the slicing or successive breaking up of bulk material into nano-sized particles. While bottom up technique means to build up a material upto nanosize by combination of atom by atom, molecule by molecule or cluster by cluster. Attrition on milling is typical example for top down method while colloidal dispersion is good example of bottom up technique [17].

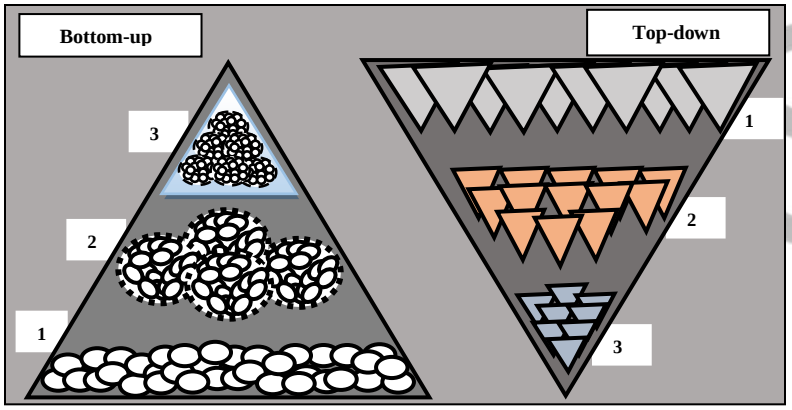

Fig. 1.1: A schematic diagram illustrating the bottom-up approach and top-down approach [18].

1.2.1 Sol- Gel Method

Bottom up concept includes different methods of preparation such as Wet chemical method, Sol-Gel method, Micro- emulsion process, hydrothermal process and Chemical vapor deposition (CVD). Sol- gel method is a typical bottom-up technique in which sol is prepared by using a metal precursor (alkoxides, acetates or nitrates) in an acidic or basic medium. This is the one of the most versatile technique generally adapted for the synthesis of metal- doped semiconductor

nanoparticle synthesis. The three main steps in the process are hydrolysis, condensation and growth formation [19]. The sol- gel approach is simple, cheap and low temperature technique that allows for the fine control of the products chemical composition. It has some advantages over other conventional methods such as good homogeneity, control grain size, particle morphology, porosity etc. [20].

1.3 Effect of temperature on crystal size

Effect of temperature on crystal growth can be explained by Ostwald's ripening phenomenon. This is the process of dissolution of small particles on heating followed by re- deposition onto larger crystals on cooling. When amorphous particles are heated, smaller particles get dissolved on heating which is followed by regrowth of crystals on remaining particles during cooling and as a result average particle size is increased. Relaxation is the cooling of crystals back to initial temperature which involves growing of particle size and is more essential for decreasing the amount of particles by increasing the particle size. Because of this Ostwald ripening the nano-crystal size can be increased by increasing its annealing temperature [21].

1.4 Characterization of Nanomaterials

Sophisticated characterization tools are used for characterization of nano-scale materials size. For example X-ray diffraction is used for the interpretation of crystalline size, crystal structure, and lattice constants of nanoparticles. Whereas, scanning electron microscope (SEM) as well as transmission electron microscope (TEM) are commonly used for the determination of size, shape and defects of nanomaterials.

1.4.1 X-ray diffraction (XRD) analysis

X- ray diffraction is a rapid analytical, non- destructive technique based on Bragg's law. It is primarily used for phase identification of a crystalline material and can provide information on sample purity, unit cell dimensions and particle size. It is the most important technique for the structure determination of crystallite.

According to Bragg's law:

$$n\lambda = 2d\sin\theta$$

Where, n is the order of reflection.

λ is the wavelength of X- rays.

θ is the Bragg's angle and

d is the inter-planar spacing [22].

The position, intensity, and the shape of diffraction peaks are main three types of information included by diffraction pattern.

XRD analysis can also be used to measure out average particle diameter of crystallite using Debye- Scherrer's formula:

$$D = \frac{k\lambda}{\beta\cos\theta}$$

Where, k is a coefficient called Scherrer's constant. (k= 0.89)

λ is the wavelength of X- rays.

β is the full at half maximum (in radian), and

θ is an angle at which peak appears [23].

1.4.2 Scanning electron microscopy (SEM)

SEM is the technique for the study of topography, surface features, and texture of nanopowders. This technique displays a three dimensional view of specimen which is very handful in examining specimens shape and structure. An electron gun emits a beam of electrons which then interacts with the surface leading to emission of electrons from the surface of the specimen during the scanning with the electron beam. The electron from the beam interacts with the sample resulting in deflection of secondary particles to a detector which subsequently converts the signals to voltage and amplifies it [24].

2. Objectives of the study

Shape and size dependent properties of TiO_2 have been well established and fabrication of these materials at nanoscale is made possible. In the past decade, many new methods have been developed for the synthesis of TiO_2 nanoparticle. However, there is great diversity about the concept of shape and size of TiO_2 nanoparticles and different researchers have presented different sizes of TiO_2 nanoparticles even at identical conditions. The main objectives of the research work presented in this paper are listed as:

- To synthesize TiO_2 nanoparticle and dope zinc ion on TiO_2 nanoparticles by sol- gel method.
- To analyze shape and size of prepared nanomaterials by X- ray diffraction and study the effect of temperature on the shape, size and structure of samples.
- To perform SEM analysis of the prepared samples.

3. Materials and Methods

3.1 Chemical reagents used

All the reactants used were of analytical grades. Zinc doped TiO_2 nanoparticles were synthesized by using titanium (IV) isopropoxide [$(C_3H_7O)_4Ti$] (97%) from Sigma Aldrich USA, zinc sulphate heptahydrate [$ZnSO_4.7H_2O$] (99.99%) from Thermo Fisher Scientific India, Ethanol [C_2H_5OH] (99.9%) from Hangshu Chemical China, Nitric acid [HNO_3] (70%) from Thermo Fisher Scientific India, Ethyl cellulose from Sigma Aldrich USA, α - Terpinol (90%) from Sigma Aldrich USA and Potassium bromide [KBr]. All the solutions of the above compounds were formed in de-ionized water.

3.2 Preparation of sample solutions

3.2.1 Preparation of 2% HNO_3 solution:

2 ml of pure HNO_3 was poured in a 100 ml volumetric flask and de-ionized water was filled

upto the mark of the volumetric flask. The solution was shaken vigorously for about 5 minutes.

3.2.2 Preparation of Zn^{2+} solution:

Molecular weight of $ZnSO_4.7H_2O$ = 287.54 g

i.e. To make 1000 ml of 1M Zn^{2+} solution 287.54 g of $ZnSO_4.7H_2O$ is required.

To make 1 ml of 1M Zn^{2+} solution 287.54/1000

=0.2875 g of $ZnSO_4.7H_2O$ is required.

3.2.2.1 100 ml of x M Zn^{2+} solution:

w g of $ZnSO_4.7H_2O$ was taken in a 100 ml volumetric flask and de-ionized water was filled upto the mark of the volumetric flask. The solution was shaken vigorously for about 5 minutes.

3.2.3 Preparation of samples

3.2.3.1 Preparation of TiO_2 nanoparticles:

For preparing TiO_2 nanoparticles by sol gel method 150 ml of absolute ethanol was poured into a 500 ml beaker and 30 ml of TTIP was mixed slowly and kept over the hot plate magnetic stirrer. 100 ml of 2% HNO_3 solution was continuously supplied to the mixture through burette. The magnetic stirrer was rotated at the speed of 700 rounds per minute (rpm) using capsule of 4 cm at room temperature for 45 minutes. At the end of stirring the solution appeared to contain white solid precipitate which was allowed to age for 24 hours in beaker covered environment. After aging for 24 hours the white ppt. of the samples were found to be settled down at the bottom of the beaker and leaving clear solution above. This clear solution was now poured off gently from the beaker leaving wet white powder which was then dried on hot air oven for 120 minutes at 100^0 C temperatures. The dried samples were then calcined for 30 minutes and grinded in mortar upto powder form and stored in a Borosilicate glass vile.

3.2.3.2 Preparation of Zn doped TiO_2 nanoparticles:

First of all 150 ml of absolute ethanol was poured into a 500 ml beaker and where 30 ml of TTIP was mixed slowly and kept over the hot plate magnetic stirrer. 100 ml of x M $ZnSO_4$ solution

and 100 ml of 2% HNO_3 solution was continuously supplied to the mixture through separate burette. The magnetic stirrer was started to rotate at the speed of 700 rounds per minute (rpm) using capsule of 4 cm at room temperature for 45 minutes. At the end of stirring the solution appeared to contain white solid precipitate which was allowed to age for 24 hours in beaker covered environment. After aging for 24 hours the white precipitate of the samples were found to be settled down at the bottom of the beaker and leaving clear solution above. This clear solution was now poured off gently from the beaker leaving wet white powder which was then dried on hot air oven for 120 minutes at 100^0 C temperature. The dried samples were then calcined for 30 minutes and grinded in mortar upto powder form and stored in a Borosilicate glass vile.

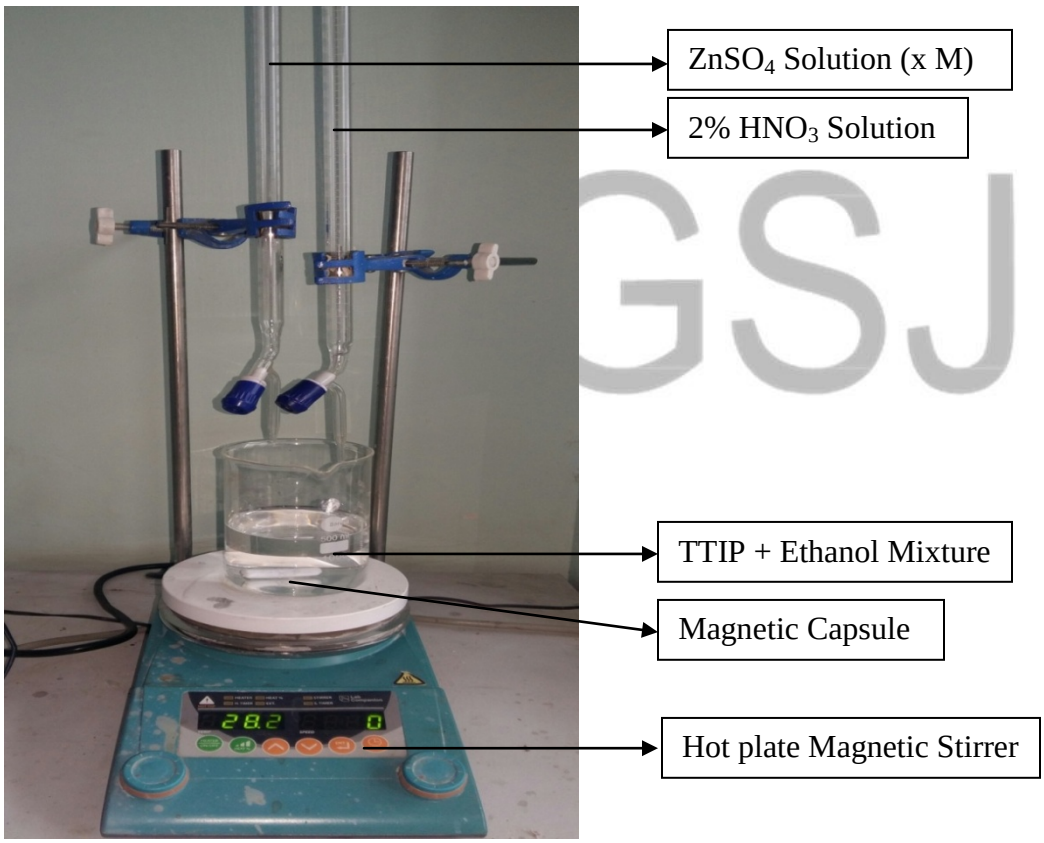

Fig 3.1: Experimental setup for the synthesis of Zn- TiO_2 nanoparticles by Sol- Gel method.

Fig 3.2: Samples collected in borosilicate glass vile for characterization.

3.3 Characterization

The characterization of the prepared samples were done by X- ray diffraction (XRD) and scanning electron microscopy (SEM).

3.3.1 X- ray diffraction:

The powdered X-ray diffraction patterns were recorded using Bruker Diffractometer with CuK_{α} radiation of wavelength (λ) = 0.15406 nm. The data was collected in continuous scan mode in the 2θ range of 20- 80 degrees for 30 minutes at 2^0 min^{-1} at the steps interval of 0.02 degrees. The X- ray generator was operated at 30 kV voltage and 10 mA tube current, which was found to be suitable for characterizing nanoparticles.

The average particle size is determined by applying Debye- Scherrer's equation:

[$D= \frac{k\lambda}{\beta \cos\theta}$]. The broadening of XRD diffraction peak profile of nanomaterials is assumed to be a convolution of pure profile and the instrumental profile. The main problem is to separate the instrumental profile from the measured diffraction pattern in order to obtain the pure physical profile containing information on the nanostructure of materials. The instrumental profile

(supplied from the XRD supplier company) was subtracted from the measured profile to get pure profile of the sample. Peak fitting was carried out using 'Origin Pro 8' software to separate the contributions from overlapping peaks and to get true FWHM values from which average particle size can be calculated.

3.3.2 Scanning electron microscope:

The field emission scanning electron microscopy was done with FEI Quanta FESEM equipment supplied with energy dispersive X- ray spectroscopy. The analysis was carried out with 10 kV acceleration voltages.

4. Results and Discussion

4.1 X- Ray diffraction analysis

While observing the XRD graph of samples in figure, it was seen that most of the sample gave peak nearly at 2θ values 25.4^0, 37.8^0, 47.95^0, 54.5^0, and 62.67^0 but some of the samples which were annealed over 500^0 C temperature gave extra peaks at 2θ values nearly 27.4^0, and 55.1^0. The peaks obtained at 2θ values 25.4^0, 37.8^0, 47.95^0, 54.5^0, and 62.67^0 are of (hkl) values as (101), (004), (200), (211), and (204) respectively indicates the presence of anatase crystal phases on prepared samples. While peaks at 2θ values nearly 27.4^0, and 55.1^0 are of (hkl) values (110) and (111) indicate the presence of rutile crystal phases of TiO_2 nanoparticles. The experimental XRD pattern agrees with the JCPDS card no 21- 1272 for anatase and 21- 1276 for rutile phase [25]. The majority of peaks are showing that majority quantity of anatase TiO_2 have been prepared during the sample preparation which may be due to low annealing temperature. For the determination of diameter of the crystals, Debye- Scherrers formula is applied picking 2θ value and full-width half maximum (FWHM) value from the mostly sharp and highest peak on the graph. The size of the samples prepared are found to be calculated as 7.09 nm, 12.32 nm, 3.90 nm, 4.25 nm, 3.23 nm, 6.70 nm, 16.67 nm, 3.04 nm, and 5.60 nm respectively in accordance with the settlement of figures below.

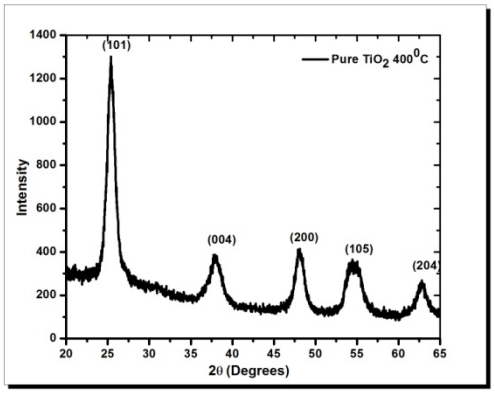

Fig 4.1 (a) Sample A_1

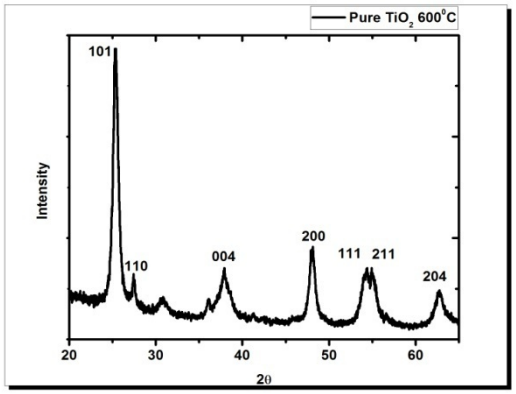

Fig 4.1 (b) Sample A_2

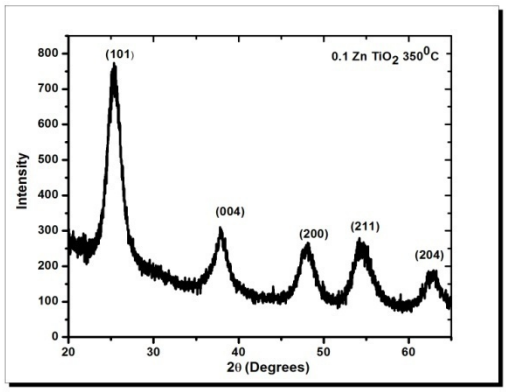

Fig 4.1 (c) Sample B_1

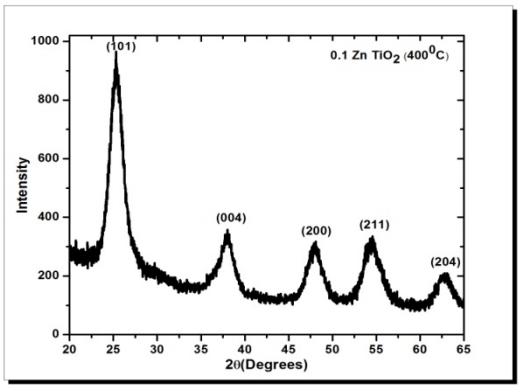

Fig 4.1 (d) Sample B_2

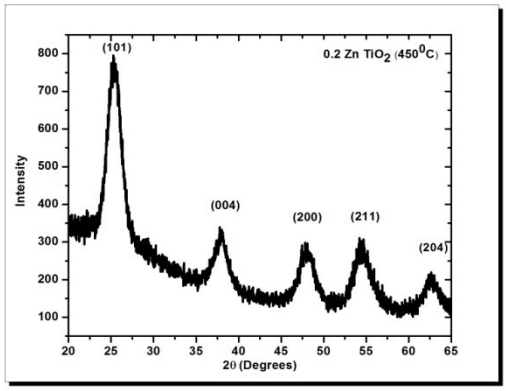

Fig 4.1 (e) Sample C_1

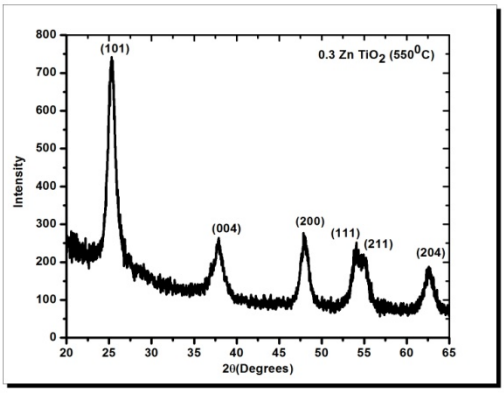

Fig 4.1 (f) Sample D_1

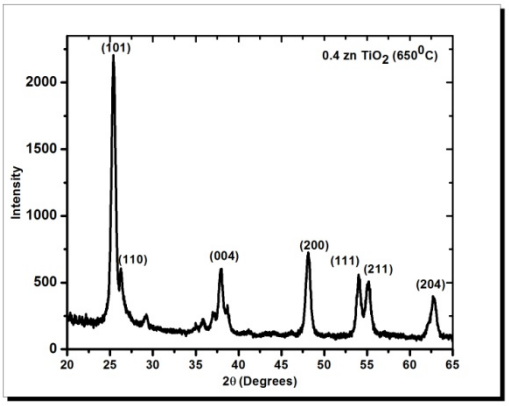

Fig 4.1 (g) Sample E_1

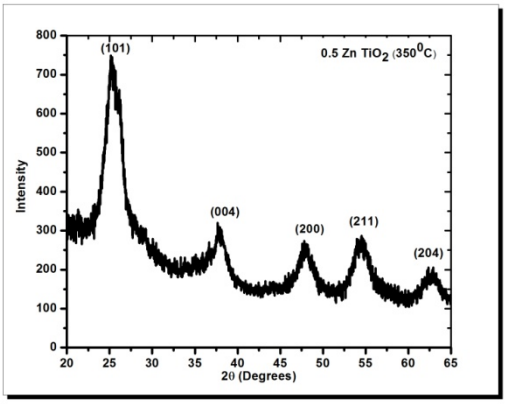

Fig 4.1 (h) Sample F_1

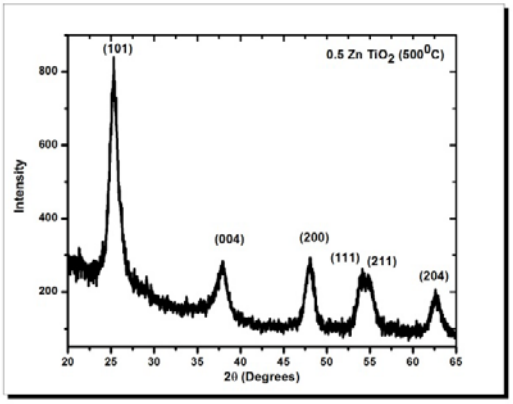

Fig4.1 (i) Sample F_2

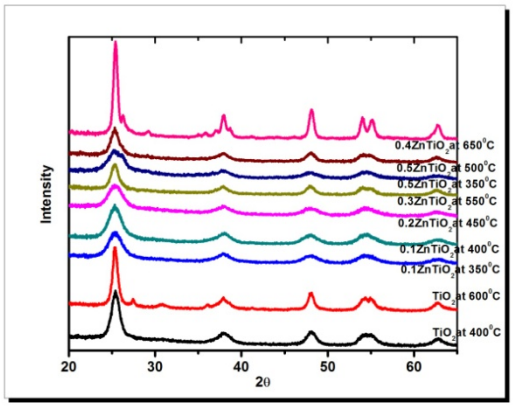

Fig4.1 (j)

Fig 4.1: XRD analysis of TiO_2 sample and different concentrated Zn doped TiO_2 samples (a) Pure TiO_2 at 400^0C (b) Pure TiO_2 at 600^0C (c) 0.1M Zn-TiO_2 at 350^0C (d) 0.1M Zn-TiO_2 at 400^0C (e) 0.2M Zn-TiO_2 at 450^0C (f) 0.3M Zn-TiO_2 at 550^0C (g) 0.4M Zn-TiO_2 at 650^0C (h) 0.5M Zn-TiO_2 at 350^0C(i) 0.5M Zn-TiO_2 at 500^0C (j) Combined XRD graph patterns.

4.2 Scanning electron microscope

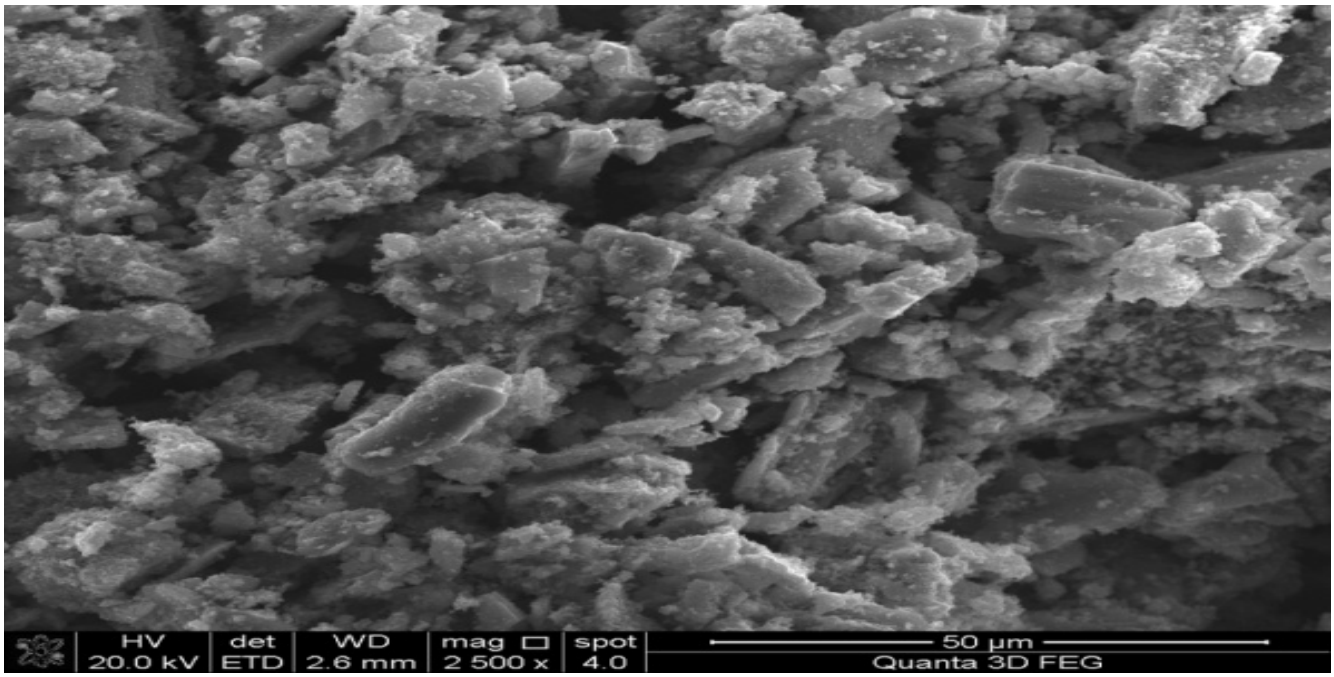

Fig 4.2 (a)

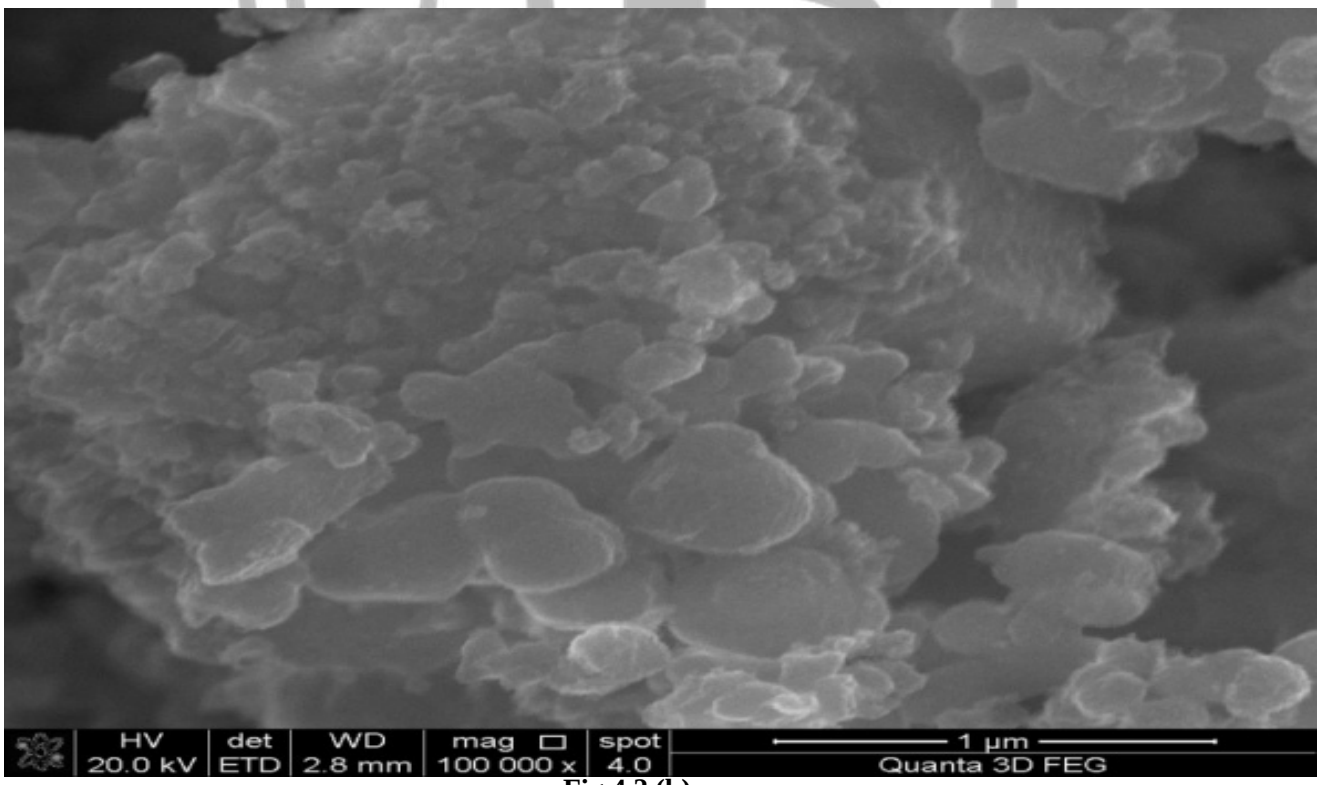

Fig 4.2 (b)

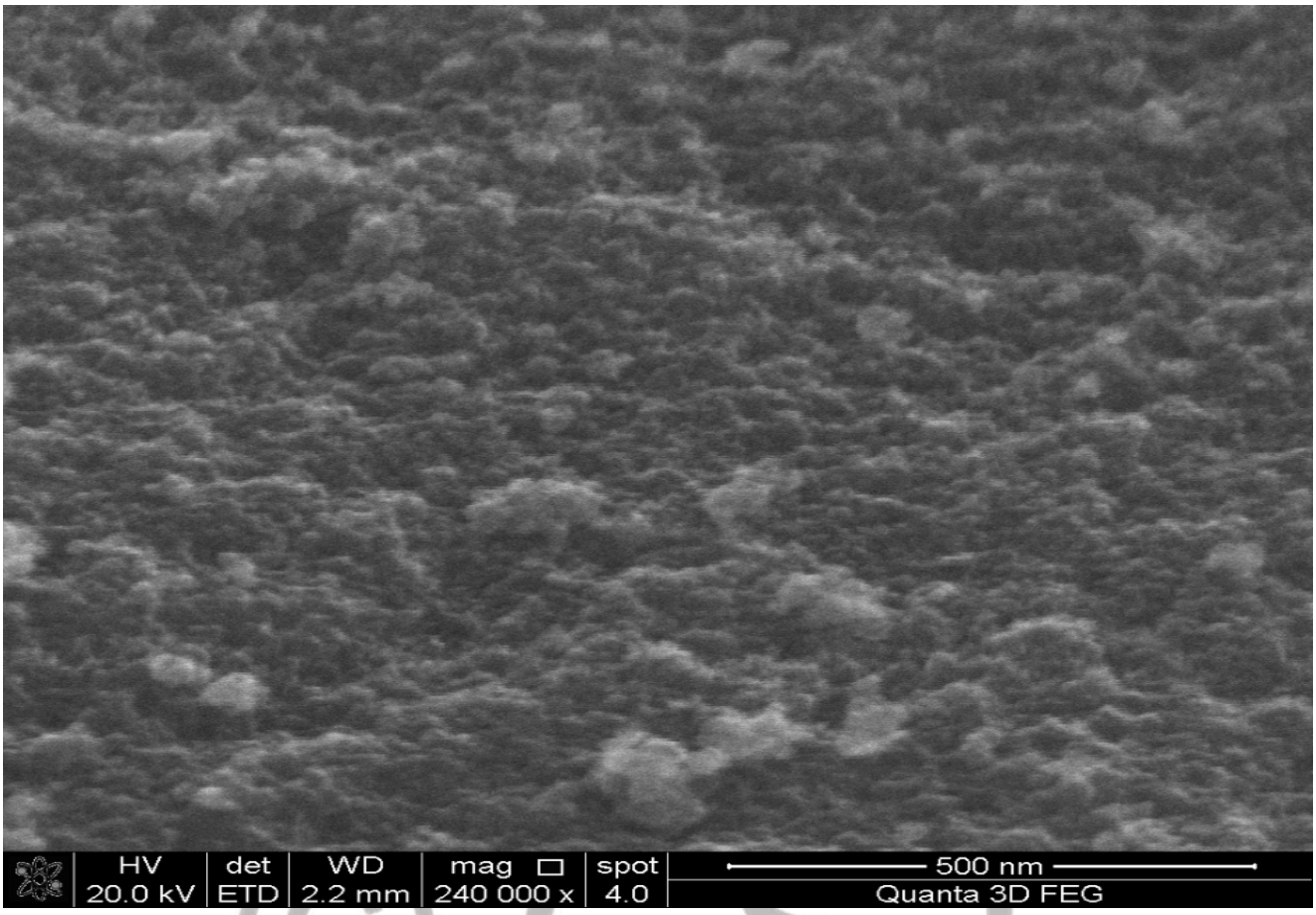

Fig 4.2 (c)

Fig 4.2: SEM images of TiO_2 samples (a) at 50 μm (b) at 1 μm and (c) 500 nm magnification

Scanning Electron Microscopic (SEM) images of TiO_2 nanoparticle sample (A_2) prepared from sol- gel methods are shown in Fig. 4.2(a), Fig. 4.2(b) and Fig. 4.2(c). SEM micrographs, shown in Fig. 4.2 (a) and Fig 4.2 (b), reveals that primary particles aggregate into secondary particles because of their small dimensions and high surface energy. Although, the diameter of these nanoparticles are difficult to determine precisely by simply viewing due to agglomeration, the average particle size from figure 4.2 (c) was estimated to be near about 11.90 nm (from isolated regions with reasonable contrasts) which is consistent with the size of same sample A_2 (12.32 nm) obtained from Debye-Scherrer's equation using XRD data.

5. Conclusions

5.1 Comparison between crystal size and annealing temperature

When we observe the relation between annealing temperature and diameter of nanocrystals, the clear dependence of size of nanoparticles on increasing temperature can be observed. These samples were annealed in different temperatures such as 350^0C, 400^0C, 450^0C, 500^0C, 550^0C, 600^0C, and 650^0C gave the nanoctystals of size 3.04nm, 4.25nm, 3.23nm, 5.60nm, 6.70nm, 12.32nm and 16.67nm respectively. When these data are compared graphically as shown in fig 5.1 below by using 'Origin 8.1', annealing temperatures were plotted at X- axis and crystal sizes were at Y-axis. According to the nature of graph obtained, crystal size has been seen increasing gradually with increase in annealing temperature. The growth of crystal size is seen increased rapidly above 550^0C because of the phase transformation of naocrystals from anatase to rutile TiO_2. These results obtained from graph is in the support to Ostwald's Ripening phenomenon and hence it can be concluded that the growth of crystal is favoured by increase in annealing temperature as a result of simultaneous dissolution of small particles followed by re-deposition into larger crystal particles. The similar nature of relation between temperature rise and crystal growth is also supported in research work of Cheng *et al* [26].

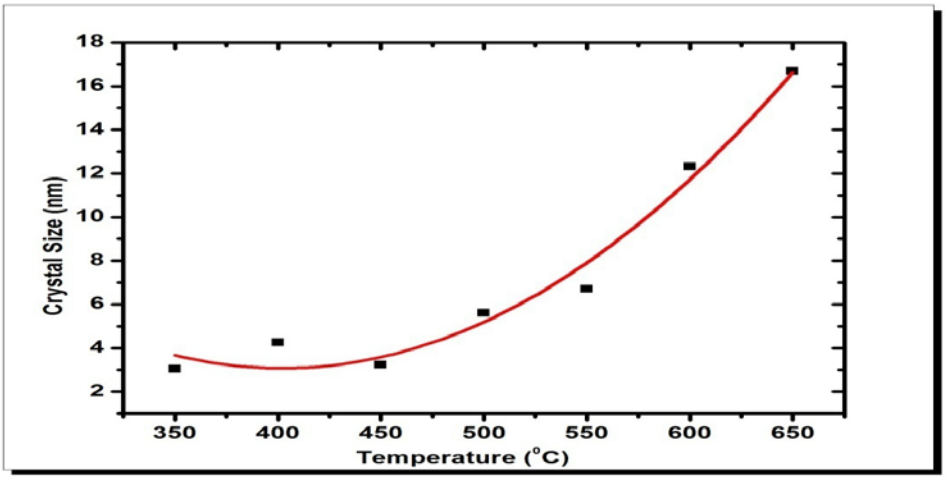

Fig 5.1: Comparison between crystal size and annealing temperature.

5.2 Phase Transformation

When we observe the peaks of samples A_2, D_1, E_1, and F_1 at fig 4.1 which were heated above 500^0C, these extra peaks at 2Ɵ values near to 27.4^0 and 55.1^0 gave *hkl* values (110) and (111) indicating the presence of rutile phases of TiO_2 nanoparticles. This experimental result indicates that anatase TiO_2 nanocrystals can be transformed into rutile TiO_2 by heating samples over 500^0C. While observing these data more precisely the average size of all samples is near to the calculated size of all samples except for samples A_2 and E_1. The larger diameter of A_2 and E_1, is due to the transformation of anatase TiO_2 into rutile TiO_2 on higher annealing temperature setup. Though samples A_2, D_1, E_1, and F_1 show the presence of rutile TiO2 nanocrystals but above 600^0C annealing temperature higher proportion of rutile TiO_2 are formed hence affecting the unusual rise in crystal diameter [27].

REFERENCES

1. Pfaff G., and Reynders P., *Chemical Rev.*, **1999**, 99, 1963.
2. Riyas S., Yasir A., and Das P. N. M., *Bull. Mater. Sci.*, **2002**, 25, 267.
3. Dhungel S. K., and Park J. G., *Renewable Energy*, **2010**, 35, 2776.
4. Wan H., Dye Sensitized Solar Cells, Literature Seminar, *The University of Alabama*, **2004.**
5. Geetha M., Singh A., Asokamani R., and Gogia A., *A Review Prog. Mater. Sci.*, **2009**, 54, 397.
6. Krol R., Goossen A., and Scoonman J., *J. Electrochem. Society*, **1997**, 20, 1723.
7. Linsebigler A., Lu G., and Yates J. T. Jr, *Chem. Rev.*, **1995**, 95, 735.
8. Gupta S. M., and Tripathi M., *Chinese Science Buletin*, **2011**, 56(16), 1639.
9. Burdett J. K., Hughbands T., Gordon J. M., Richardson J. W. Jr, and Smith J. V., *J. American Chem. Soc.*, **1987**, 109, 3639.
10. Coronado D. R., Gattorno G. R., Pesquera M. E. E., Cab C., Coss R., and Oskam G., *Nanotechnoogy*, **2008**, 19.

11. Zhang H., and Banfield J. F., *Am. Mineral*, **1999**, 84, 528.

12. Li W., Ni C., Lin H., huang C. P., and Shah S. I., *J. App. Physics*, **2004**, 96, 6663.

13. Kominami H., Kohno M., and Kera Y. J., *Mater. Chem.*, **2000**, 10, 1151.

14. Cheng P., Zheng M., Jin Y., Gu M., and Huang Q., *Mater. Lett.*, **2003**, 57, 2989.

15. Xiong G., Wang X., Lu L., Yang X., and Xu Y., *J. Solid State Chem.*, **1998**, 141, 70.

16. Chen C. J., and Wu J. M., *Mater. Sci. Eng*., ***1990***, *B5, 377.*

17. Byranvand M. M., Kharat N., Fatholahi L. and Beiranvand Z. M., *Journal of Nanostructures*, **2013**, 3, 1.

18. Meyers M. A., Mishra A. and Benson D. J., *Progress of Materials Science*, **2006**, 51, 427.

19. Burda C., Chen X., Narayan R., and El- Sayed M. A., *Chemical Reviews*, **2005**, 15, 1025.

20. Rajput N., *Internatonal Journal of Advances in Engineering and Technology*, **2015**, 7(4), 1809.

21. Westen T. V., and Groot R. D., *Cryst. Growth and Des*., **2018**, 18, 4952.

22. Koirala D., Study on Influence of Precursor Sources and Concentration Size and Crystalline Structure of Cadmium telluride Nanoparticles, M. Sc. Thesis Dissertation, *Tribhuvan University*, **2016**.

23. Dorofeev G. A., Streletskii A. N., Povstugar I. V., Protasov A. V., and Elsukov E. P., *Colloid Journal*, **2012**, 74, 675.

24. Goldstein J., Newbury D. E., Joy D. C., Lyman C.E., Echlin P., Lifshin E., Sawyer L., and Michael J. R., *Scanning Electron Microscopy and X-ray Microanalysis*, Springer, 3rd Edition, **2007**,21.

25. Mulmi D. D., Thapa D., Dahal B., Baral D., and Solanki P. R., *Int. Journals of Materials Science and Engineering*, **2016**, 4, 172.

26. Cheng H., Ma J., Zhao Z., and Qi L., *Chemical Mater*., **1995**, 7, 663.

27. Horng M., Yin X., and Yang H., Poster Presentation, *University of Rochester*, **2011**.